Journal Name

ARTICLE TYPE

Vapour-Liquid Interfacial Properties of Square-Well chains from Density Functional Theory and Monte Carlo Simulation

Francisco José Martínez-Ruiz,[a] Felipe J. Blas,*[a] A. Ignacio Moreno-Ventas Bravo,[b] José Manuel Míguez[a] and Luis G. MacDowell[c]

The statistical associating fluid theory for attractive potentials of variable range (SAFT-VR) density functional theory (DFT) developed by [Gloor *et al.*, J. Chem. Phys., 2004, **121**, 12740-12759] is used to predict the interfacial behaviour of molecules modelled as fully-flexible square-well chains formed from tangentially-bonded monomers of diameter σ and potential range $\lambda = 1.5\sigma$. Four different model systems, comprising 4, 8, 12, and 16 monomers per molecule, are considered. In addition to that, we also compute a number of interfacial properties of molecular chains from direct simulation of the vapour-liquid interface. The simulations are performed in the canonical ensemble, and the vapour-liquid interfacial tension is evaluated using the wandering interface (WIM) method, a technique based on the thermodynamic definition of surface tension. Apart from surface tension, we also obtain density profiles, coexistence densities, vapour pressures, and critical temperature and density, paying particular attention to the effect of the chain length on these properties. According to our results, the main effect of increasing the chain length (at fixed temperature) is to sharpen the vapour-liquid interface and to increase the width of the biphasic coexistence region. As a result, the interfacial thickness decreases and the surface tension increases as the molecular chains get longer. The interfacial thickness and surface tension appear to exhibit an asymptotic limiting behaviour for long chains. A similar behaviour is also observed for the coexistence densities and critical properties. Agreement between theory and simulation results indicates that SAFT-VR DFT is only able to predict qualitatively the interfacial properties of the model. Our results are also compared with simulation data taken from the literature, including the vapour-liquid coexistence densities, vapour pressures, and surface tension.

[a] *Laboratorio de Simulación Molecular y Química Computacional, CIQSO-Centro de Investigación en Química Sostenible and Departamento de Ciencias Integradas, Universidad de Huelva, 21007 Huelva, Spain.*

[b] *Laboratorio de Simulación Molecular y Química Computacional, CIQSO-Centro de Investigación en Química Sostenible and Departamento de Ciencias de la Tierra, Universidad de Huelva, 21007 Huelva, Spain.*

[c] *Departamento de Química Física, Facultad de Ciencias Químicas, Universidad Complutens, 28040 Madrid, Spain.*

* *Corresponding author, e-mail: felipe@uhu.es*

1 Introduction

Interfacial phenomena play a key role not only in many scientific fields, such as nucleation, nanotechnology or the dynamics of phase transitions, but also in a great number of practical applications[1]. Solubilization of immiscible fluids, detergency, lubricants, and the design of lyotropic liquid-crystalline amphiphiles for use as soaps, cosmetics and foodstuffs are some common applications where an understanding of the interfacial properties is essential.

Apart from experiments, which allow to determine in a straightforward manner the interfacial properties of a give real system, theoretical and computational methods based on Statis-

tical Mechanics are also key tools for studying this kind of properties. In fact, microscopic models have played and still are playing an essential role in understanding the thermodynamic and interfacial properties of real and model complex fluid systems. These methodologies allow to understand, from a molecular perspective, which microscopic parameters determine the interfacial properties of macroscopic systems. Since molecular models are based on the knowledge of a given intermolecular interaction potential, calculations obtained from computer simulations, that provide a nearly exact solution of the problem, can be compared with predictions obtained from more or less complex theoretical approaches. This comparison usually helps to understand the complex interfacial behaviour of an important number of systems.

Although real systems are usually investigated due to its industrial and practical interest, simple model systems are also studied since provide an insight on how molecular details determine the behaviour of a given system. In fact, new theoretical frameworks are usually developed in a first stage for these kind of systems. This allows to implement more elaborated and complex theories that in a second stage could be apply to predict the thermodynamic and interfacial behaviour of real models. From a molecular perspective, Monte Carlo and molecular dynamics computer simulation techniques and theoretical approaches based on Statistical Mechanics have demonstrated to be key methodologies for studying the interfacial properties of fluids and fluid mixtures. Particularly interesting in this context are simple molecular models, such as chain-like systems. However, it is key for this perspective to know accurately the behaviour of these systems and to compare results from computer simulation to validate theoretical approaches.

Apart from simple spherical models, during the last two decades the interfacial properties of molecular model systems have been investigated using both Monte Carlo and molecular dynamics techniques of a number of systems interacting through different intermolecular potentials, mostly LJ and Mie[2–15], but also systems that interact via the hard-core Yukawa potential[16–20], and the square-well (SW) potential[5,9,17,21–28]. In fact, whereas the computation of interfacial properties of polymer models have been the subject of a number of recent papers,[29–33] results for the well known fully-flexible SW model, in which square-well segments (monomers) of diameter σ and potential range λ are tangentially bonded to form molecular chains are scarce. In particular, computer simulation results for determining the vapour-liquid phase equilibrium of chain like molecules formed from spherical units that interact through the SW intermolecular potential have received relatively less attention than other systems. As we have mentioned before, accurate knowledge of the interfacial properties of molecular model systems is essential to check if sophisticated Statistical Mechanics approaches[34], such as Density Functional Theory (DFT)[1,35–39] and Square Gradient Theory

(SGT)[40,41] are able to predict with confidence the interfacial behaviour of these models.

Escobedo and de Pablo[42] determined the vapour-liquid phase equilibrium of fully-flexible tangent square-well chains (TSWC) formed from tangentially bonded monomers with SW interactions comprising of 4, 8, 16, 32, and 100 monomers per molecule using the Gibbs Ensemble Monte Carlo (GEMC) technique. Three years later, Hu et al.[43] obtained the vapour-liquid equilibrium from Molecular Dynamics (MD) simulations of vibrating square-well chains (VSWC) formed from 2, 4, and 8 SW monomers with three different average bond lengths, $l = 0.97$, 0.60, and 0.40σ. The model was originally introduced by Rapaport in late 1970s and early 1980s. The two first models correspond to freely-jointed or fully flexible chains, and the last one ($l = 0.40\sigma$) corresponds to chains with average bond angles constrained to $127°$ (see the work of Hu et al.[43] for further details). Although both models seem to be similar, an important difference exists between them. In the case of the model simulated by Escobedo and de Pablo (TSWC), the bond length between consecutive bonded monomers is strictly equal to $l = \sigma$, the diameter of the segments forming the chains, and hence, the monomers are tangentially bonded. In the second case, corresponding to the model simulated by Hu et al., the bond length between monomers is not constant but varies in all cases $\pm 0.03\sigma$ around an average bond length (0.97, 0.60, and 0.40σ).

More recently, Chapela and Alejandre[24] have determined the vapour-liquid interfacial properties of VSWC of 2, 4, 8, and 16 monomers with the same average bond length that those considered by Hu et al. In particular, they have obtained the vapour-liquid coexistence densities, vapour pressure, interfacial thickness, and surface tension simulating directly the vapour-liquid interface using MD computer simulation. Initially, the vapour-liquid phase equilibrium of VSWC model seems to be equivalent to that of the TSWC model since the beads of VSWC with bond lengths $l = 0.97\sigma$ are nearly tangentially bonded. However, as pointed by Hu et al., the VL coexistence curves of VSWC are shifted to higher temperatures relative to those of fully flexible SW chains with monomers tangentially bonded. In particular, they compare their original data with those obtained by Escobedo and de Pablo corresponding to truly tangentially bonded chains. As can be seen in Fig. 3 of the paper from Hu et al.[43], the coexistence curves corresponding to VSWC with average bond length $l = 0.97\sigma$ are systematically higher that those corresponding to the TSWC model. Hu et al. attribute the differences between both results to differences in the compressibility factors of both models, which have a significant effect on the phase behaviour: the VSWC have lower compressibility factor due to its non-stiff bonds that make it more flexible.

The work of Chapela and Alejandre is a nice extension of the seminal work of Hu et al. in the characterisation of thermody-

namic properties of VSWC since they extend the study to deal with the interfacial properties of the same system. However, conclusions from Chapela and Alejandre concerning VSWC with average bond length $l = 0.97\sigma$ are in disagreement with those found by Hu *et al.* The ensuing discussion shows that is not clear that thermodynamic, and especially interfacial properties of VSWC with bond length $l = 0.97\sigma$ must be equivalent to those of TSWC with $l = \sigma$. The obvious way to elucidate this point is to calculate the interfacial properties of the specific model in which l, the bond length between consecutive monomers, is strictly constant.

As we have mentioned previously in this Section, it is possible to determine the interfacial properties of molecular model systems, not only from computer simulation but also using a molecular theory based on Statistical Mechanics. Apart from the parachor of MacLeod[44] and the corresponding states principle of Guggenheim[45], which are empirical approaches widely used that provide a very accurate description of the interfacial tension of complex substances, the Square Gradient Theory (SGT) is one of the most popular methodologies for the theoretical description of interfacial systems based on a microscopic point of view. The approach, originally proposed by van der Waals in its theory of inhomogeneous fluids[40], and rediscovered by Cahn and Hilliard several decades after[41], is based on a Taylor series of the Helmholtz free-energy density in terms of the density profile. This method is very popular since only two ingredients are necessary: an equation of state for the bulk fluid (first-order contribution) and the value of the so-called influence parameter, which enters in the theory in the square-gradient term of the series (second-order contribution). The later is, however, the main limitation of the SGT formalism since in practical applications is adjusted by fitting to the experimental interfacial-tension data of a great number of complex substances and their mixtures, including hydrocarbons, carbon dioxide, water, and their mixtures[14,46–62].

However, one of the most sophisticated and successful theoretical treatments for the study of interfacial phenomena is DFT. This approach is entirely predictive with no adjustable parameters[1,39]. Most of the different versions presented in the literature have the same common point: the free-energy density functional is divided in two parts, a reference term that incorporates only, apart from the ideal contribution, the short-range interactions, and a perturbative term accounting for the long-range interactions. The reference term can be treated under the local density approximation (LDA) or a weighted-density approximation (WDA)[1,39]. Several authors have proposed different functions and approaches[63–71], including those that incorporate correlations in the perturbative contribution[71–75] following similar ideas to those originally proposed by Toxvaerd[76–78].

Few years ago, Gloor *et al.*[72,73,79,80] and Llovell *et al.*[81,82] proposed a DFT approach in which the well-known SAFT formalism for potentials of variable range (SAFT-VR) is incorporated to de-

scribe the interfacial properties of molecular substances and their mixtures, including alkanes, carbon dioxide, and water. In particular, the theoretical formalism uses a Helmholtz free-energy functional which reduces to the SAFT-VR[83,84] free energy of the homogeneous fluid in the limit of constant density. SAFT-VR is one of the variants of the original SAFT equation of state[85–94] based on Wertheim's first-order thermodynamic perturbation theory for associating systems[95–100]. In this approach, the free energy is a sum of different microscopic contributions (the ideal, hard-sphere, dispersion, chain, and association contribution). This version has already shown to accurately represent the vapour-liquid and liquid-liquid phase equilibrium of mixtures of model and real complex substances and their mixtures. This is a key point since one of the most important requirements for an accurate description of the interfacial properties of inhomogeneous systems with a DFT treatment is that the properties of coexisting homogeneous bulk phases are described reliably.

The aim of this paper is threefold: (1) to determine the interfacial properties, with special emphasis on the vapour-liquid surface tension, of fully-flexible chains formed from tangentially bonded monomers interacting through the SW intermolecular potential by direct coexistence (TSWC model); (2) to calculate the interfacial properties of the same model with the SAFT-VR DFT formalism to check the accuracy of the theory in predicting the interfacial properties of SW chains, including density profiles and surface tension; and (3), to compare the simulation results of the TSWC model with bond length $l = \sigma$, with those obtained by Chapela and Alejandre for the VSWC model with $l = 0.97\sigma$. This will allow to know if both models are completely equivalent. To our knowledge, this is the first time the interfacial properties of the TSWC model are studied from computer simulation. In addition to that, it is also the first time the predictions from the SAFT-VR DFT formalism are compared with simulation data.

The rest of the paper is organised as follows: In then next section we briefly consider the molecular model and the theory used in this work. After this, we present the simulation details section and the results obtained in this work. In the final section we present the main conclusions.

2 Model and Theory

The molecular model and theory used to determine the bulk phase behaviour and the interfacial properties of TSWC are briefly described in this section before presenting the results.

The molecular chains considered in this work are formed from m spherical segments (monomers) tangentially bonded that interact through the SW intermolecular potential, which is characterised by a diameter σ, a dispersive energy ε, and a potential range λ. The chains are fully flexible, i.e., the model does not consider neither bending nor torsional potentials between the segments that form the chains. However, we account for in-

tramolecular interactions between monomer of the same chain separated by more than one bond. This crude model takes into account the main attributes of the molecular architecture of the chain, including segment connectivity, that represent topological constrains and internal flexibility, excluded volume effects, and attractive interactions between the different segments that form the molecules.

The SW potential between two segments, in the same or in different molecules, is given by:

$$\phi_{ij}(r_{ij}) = \begin{cases} \infty & r_{ij} \leq \sigma \\ -\varepsilon & \sigma < r_{ij} \leq \lambda\sigma \\ 0 & r > \lambda\sigma \end{cases} \tag{1}$$

where r_{ij} denotes the distance between the centres of the two segments, and $\lambda\sigma$ is the range of the dispersive interaction of depth ε.

The interfacial properties of selected SW chains formed from different number of monomers are considered within the context of the SAFT-VR DFT formalism, a DFT based on the SAFT-VR free energy. In what follows, we give a brief summary of the theory since further details can be found in references [1,39,101].

In an open system of volume V, at temperature T, and chemical potential μ, in absence of external fields, the grand potential functional $\Omega[\rho(\mathbf{r})]$ is given by[1],

$$\Omega[\rho(\mathbf{r})] = F[\rho(\mathbf{r})] - \mu \int d\mathbf{r}\,\rho(\mathbf{r}) \tag{2}$$

where $F[\rho(\mathbf{r})]$ is the intrinsic Helmholtz free energy functional, and $\rho(\mathbf{r})$ is the density profile. The minimal value of $\Omega[\rho(\mathbf{r})]$ is the equilibrium grand potential of the system, and the corresponding equilibrium density profile, $\rho_{eq}(\mathbf{r})$, satisfies the corresponding Euler-Lagrange condition[1],

$$\left.\frac{\delta\Omega[\rho(\mathbf{r})]}{\delta\rho(\mathbf{r})}\right|_{eq} = \left.\frac{\delta F[\rho(\mathbf{r})]}{\delta\rho(\mathbf{r})}\right|_{eq} - \mu = 0 \tag{3}$$

According to the perturbative scheme of the SAFT-VR DFT treatment, the free energy is expressed into reference, $F^{\text{ref}}[\rho(\mathbf{r})]$, and perturbative attractive, $F^{\text{att}}[\rho(\mathbf{r})]$, terms[72,73,81,82],

$$F[\rho(\mathbf{r})] = F^{\text{ref}}[\rho(\mathbf{r})] + F^{\text{att}}[\rho(\mathbf{r})] \tag{4}$$

The reference takes into account all of the contributions to the free energy due to short-range interactions according to the following expression[72,73,81,82]

$$F^{\text{ref}}[\rho(\mathbf{r})] = F^{\text{ideal}}[\rho(\mathbf{r})] + F^{\text{hs}}[\rho(\mathbf{r})] + F^{\text{chain}}[\rho(\mathbf{r})] + F_2[\rho(\mathbf{r})] \tag{5}$$

Here, F^{ideal} is the ideal-gas contribution. The term F^{hs} is the (residual) contribution for an inhomogeneous system of hard spheres resulting form the repulsive interactions between monomers. This contribution is treated within a Local Density Approximation (LDA)[1,39], which implies that the hard-sphere contribution to the free energy of the inhomogeneous system is approximated by that of an equivalent homogeneous system of hard spheres evaluated at the local density $\rho(\mathbf{r})$. There are many different DFT versions in the literature that predict the interfacial behaviour of pure and liquid mixtures[70,71,102], and other more sophisticated that include Non-Local Density Approximations (NLDA)[66–68,74,101,103–105] or even take into account explicitly the fluctuations of the system close to the critical point[75]. The use of a LDA is fully justified in the case of planar vapour-liquid interfaces, in which only smooth variations of the density profile exist[1]. F^{hs} is given by the Carnahan and Starling[34,106] expression for the residual free energy of the homogeneous hard-sphere system. The term F^{chain} in Eq. (5) corresponds to the contribution to the free energy due to the formation of chains of m square-well segments, according to the standard Wertheim's first-order thermodynamic perturbation theory (TPT1) of association[86]. Also note that this contribution is treated at the LDA level as the interactions they represent are short range in nature. Finally, the last contribution F_2 in Eq. (5) corresponds to the second-order term in a Barker and Henderson[107] high-temperature perturbation expansion of the free energy. As it is well explained in the original paper[72], this term is incorporated in order to recover the SAFT-VR free energy of the homogeneous bulk phases, and is also treated at the LDA level. The full formulas for the excess free energy contributions are given in the Appendix.

The perturbative term F^{att} in Eq. (4) includes the contributions resulting from the attractive square-well interactions between the monomeric segments. In our approach this is given by[1,39,70]

$$F^{\text{att}}[\rho(\mathbf{r})] = \frac{1}{2}\int d\mathbf{r}\,m\rho(\mathbf{r})\int d\mathbf{r}'\,m\rho(\mathbf{r}')\,g^{\text{ref}}(\mathbf{r},\mathbf{r}';\rho(\mathbf{r}),\rho(\mathbf{r}'))\,\phi^{\text{att}}(|\mathbf{r}-\mathbf{r}'|), \tag{6}$$

Here g^{ref} is the pair distribution function of the hard-sphere reference system and ϕ^{att} is the attractive part of the segment-segment square-well potential. As little is known of the pair distribution function of the inhomogeneous hard-sphere fluid, we approximate this function by the pair distribution function of a homogeneous system of hard spheres evaluated at a mean density defined as $\bar{\rho} = (\rho(\mathbf{r}) + \rho(\mathbf{r}'))/2$. In order to be consistent to the SAFT-VR original treatment of the bulk fluid[83], the pair distribution function can be further approximated by its value at contact for an equivalent system with an effective density $\bar{\rho}_{\text{eff}}$ (which is a function of the original density ρ and the range λ of the potential[72,83]). The final expression of the perturbative dispersive term used in the SAFT-VR DFT approach is given by

$$A^{\text{att}}[\rho(\mathbf{r})] = \frac{1}{2}\int d\mathbf{r}\,m\rho(\mathbf{r})\int d\mathbf{r}'\,m\rho(\mathbf{r}')\,g^{\text{hs}}(\sigma;\bar{\rho}_{\text{eff}})\,\phi^{\text{att}}(|\mathbf{r}-\mathbf{r}'|). \tag{7}$$

Within this approach, the free energy given by Eq. (4) reduces to the bulk SAFT-VR expression for homogeneous systems[83] when $\rho(\mathbf{r})$ is the bulk average number density ρ.

As we have mentioned previously, the equilibrium density profile follows from the solution of the Euler-Lagrange Eq. (3). In this study we consider planar vapour-liquid interfaces (which are assumed to be perpendicular to the z axis) and thus $\rho(\mathbf{r}) \equiv \rho(z)$, where z is the distance normal to the interface. As in our previous papers[72,72,82], a numerical integration of Eq. (3) is performed by starting from a trial density profile ρ_{old} with limiting densities which correspond to the vapour and liquid equilibrium bulk densities (obtained as described in reference[83]). This results in a new density profile ρ_{new} and the process is repeated using a standard iterative scheme until the full density profile changes by no more than a specified tolerance.

Once the equilibrium density profile $\rho_{eq}(z)$ is known, the surface tension can be determined from the simple thermodynamic relation

$$\gamma = \frac{\Omega + PV}{\mathscr{A}} \qquad (8)$$

where $\mathscr{A}$ is the interfacial area and P is the bulk pressure.

3 Simulation Details

In this work, we determine the phase equilibrium and interfacial properties of chain molecules formed from spherical monomers that interact through the SW intermolecular potential from Monte Carlo simulation. The use the same model presented in the previous section to predict the interest properties of representative chain molecules from the SAFT-VR DFT and Monte Carlo simulation. Results from both approaches are compared in the next section in order to determine the ability of the theoretical formalism in predicting both phase equilibrium and interfacial properties.

The number of molecules, N, used in each simulation depends on the chain length. We consider $N = 504, 252, 168$, and 126 for systems formed by 4, 8, 12, and 16 monomers, respectively. This choice is made so as to have systems with the same total number of monomers irrespective of the particular chain length.

A code for the simulation of LJ dumbbells[108] has been extended to deal with the simulation of either rigid or chain molecules in the NVT, NPT or grand canonical ensemble in either bulk or a slit-pore geometry, including not only molecules interacting through the LJ potential, but also the SW intermolecular potential. Translational and rotational movements are supplemented with configurational bias displacements[109–111] and deletion/insertion attempts.[112] The energy is evaluated efficiently with the help of a link cell list. Further details on the specific implementation of configurational bias displacements and the cell list may be found elsewhere.[113]

Simulations are performed in the NVT ensemble. We consider a system of N molecules at a temperature T in a volume $V =$ $L_x L_y L_z$, where L_x, L_y and L_z are the dimensions of the rectangular simulation box. A homogeneous liquid system is first equilibrated in a rectangular simulation box of dimensions $L_x = L_y = 11\sigma$, and $L_z = 24, 26, 28$, and 30σ for systems with LJ chains formed by 4, 8, 12, and 16 monomers, respectively. In the case of fully-flexible chains the end-to-end dimension of the chains is of the order of $\sim m^{1/2}$, which for the longest chains of $m = 16$ studied corresponds to 4σ. The box is then expanded to three times its original size along the z direction, while leaving the liquid phase at the centre. On performing this expansion, care must be taken not to break chains spanning the periodic boundary conditions of the initial configuration. As a result, we obtain a centred liquid slab with those chain bits spanning across the boundary conditions of the original liquid configuration protruding into empty boxes of equal size at each side. The final overall dimensions of the vapour-liquid-vapour simulation box are therefore $L_x = L_y = 11\sigma$, and $L_z = 72, 78, 84$, and 90σ for the corresponding chain lengths.

All simulations are organised in cycles, where each cycle corresponds to N trial MC moves. Our MC procedure comprises three types of configurational updates: one involving a trial displacement of the molecular centre of mass, and the other two, a partial and complete molecular regrowth of the molecular chains. For the latter type of moves, we consider a configurational bias scheme. Each type of move is chosen with a probability of 20, 40, and 40%, respectively. The magnitudes of the appropriate displacements are adjusted so as to get an acceptance rate of $\sim 30\%$ to 50%. We use periodic boundary conditions in all three directions of the simulation box.

Calculation of the coexistence pressures, from a Monte Carlo simulation perspective, poses some difficulties. For a model of fixed bond lengths as the one studied here, the expression for the virial is awkward, particularly for long chains whose end to end distance may be larger than half the simulation box[114]. This problem notwithstanding, acquisition of meaningful averages for such low pressures as are typical well below the critical point requires very lengthy simulations. For that reason, we calculate the pressure by means of a thermodynamic integration hinted at previously.[115] In this procedure we exploit the Gibbs–Duhem equation, $dp = \rho d\mu$, at constant temperature. By splitting the chemical potential into ideal gas and residual contributions, and integrating by parts, we obtain:

$$\beta p(\rho) = \rho - \int_0^\rho \left[\mu_r(\rho') - \mu_r(\rho) \right] d\rho' \qquad (9)$$

In order to exploit this equation for the calculation of the pressure, we performed a series of bulk simulations in the Grand–Canonical ensemble. As in the case of the inhomogeneous system, we also organise these simulations in cycles. As before, each cycle consists in N trial MC moves. The only difference is that we do not perform full chain configurational bias regrowth but

Grand–Canonical configurational bias chain insertion/deletion. Each type of move is chosen with a probability of 20%, 40%, and 40% for centre of mass displacements, partial configurational bias chain regrowth, and Grand–Canonical configurational bias chain insertion/deletion, respectively. Typically, we run between 10 and 20 thermodynamic states from the ideal gas limit to the supersaturated vapour. Each state is equilibrated for 10^6 MC cycles, and averages of density are determined over a further period of 8×10^6 MC cycles. The production stage is divided into M blocks. We consider $M = 50$ for all the states (different chemical potentials and temperatures) and chain lengths considered here. With this choice, the density at each chemical potential has been obtained from an average of 50 uncorrelated or statistically independent blocks (1.6×10^5 cycles per block). The residual chemical potential, as a function of density, was then fitted to a polynomial of 2nd up to 5th order and integrated up to the coexistence vapour density. We have checked that our fitting procedure is essentially independent of the degree of the polynomial fit. Once the function $\mu_r = \mu_r(\rho)$ has been obtained, the vapour pressure can be readily calculated from Eq. (9). The statistical uncertainty associated with the thermodynamic integration of the equation of state given in Eq. (9) has been estimated from the *synthetic analysis* proposed recently by de Miguel[116], and applied by MacDowell and Blas[117] to determine the vapour pressure of TSWC formed from different numbers of LJ monomeric units. In this particular case, we have generated 10^6 synthetic data sets according to the de Miguel's prescription,[116] obtaining a Gaussian-like distribution for the vapour pressure at each temperature.

The computation of the surface tension is accomplished with the use of the Wandering Interface Method (WIM) proposed by MacDowell and Bryk several years ago[9]. The WIM technique is an extension of the NPT ensemble in which the interfacial area is allowed to fluctuate at random. This is achieved by introducing a new MC move, which consists of an attempt to deform the box by changing the interfacial area of the system at constant volume. The attempted moves are accepted according to the usual canonical rules, and the surface tension may be extracted from the resulting surface area probability distribution. Further details can be found in Ref.[9] The WIM approach can also be implemented in the grand canonical ensemble (suitable for confined fluids against a wall) or in the canonical ensemble; the latter is a better option for the description of vapour-liquid or liquid-liquid interfaces. For the special case of discrete sampling of the surface area, the WIM technique becomes equivalent to the recent expanded ensemble methodology.[8,21]

For each chain length, we perform simulations of inhomogeneous systems at different temperatures where vapour-liquid equilibrium is expected. We typically consider either six or seven temperatures in the range $\sim 0.5\,T_c$ up to $\sim 0.9\,T_c$, where T_c is the critical temperature of the system. Each series is started at the

lowest temperature studied. This system is well equilibrated for 10^7 MC cycles, and averages are determined over a further period of 1.6×10^8 MC cycles. The production stage is divided into M blocks. The ensemble average of the surface tension is given by the arithmetic mean of the block averages and the statistical precision of the sample average is estimated from the standard deviation in the ensemble average from $\overline{\sigma}/\sqrt{M}$, where $\overline{\sigma}$ is the variance of the block averages and $M = 80$, but in some cases averages are taken over more blocks.

All the quantities in our paper are expressed in conventional reduced units, with σ and ε being the length and energy units, respectively. Thus, the temperature is given in units of ε/k_B, the densities in units of σ^{-3}, pressure in units of ε/σ^3, the surface tension in units of ε/σ^2, and the interfacial thickness and potential range in units of σ.

4   Results

We apply the SAFT-VR DFT approach outlined in the Introduction to study the vapour-liquid interfacial properties of fully-flexible TSWC with potential range $\lambda = 1.5\sigma$ and varying chain length. In addition to that, we also present simulation data of the exactly same model and compare both results to asses the accuracy of the theoretical formalism used in this work. We focus mainly on the interfacial properties of chain like models interacting through the SW intermolecular potential, such as density profiles and interfacial tension. We are particularly interested in the dependence of these interfacial properties with the chain length of the system.

As in previous works, we also use the bulk SAFT-VR equation of state to determine the vapour-liquid equilibrium, including the coexistence curves and vapour pressure, as functions of temperature. This allows to check if the theory is able to predict accurately, not only the behaviour of the system at the interface, but also the equilibrium properties. Since simulation data for the interest properties of the exactly same model (studied previously by Escobedo and de Pablo[42]) and nearly the same model (studied by Hu *et al.*[43] and more recently by Chapela and Alejandre[24]) exist in the literature, as outlined in the Introduction, we also compare the theoretical predictions and simulation data obtained in this work with previous simulation results. It is worthy of special mention that interfacial properties are very sensitive to molecular details. Comparison between predictions obtained from similar but not identical models allows, such as in the case of the TSWC and VSWC models, to check if these differences provoke different macroscopic interfacial behaviour.

We use the SAFT-VR formalism, including the bulk limiting equations as well as the full SAFT-VR DFT approach, to calculate the equilibrium properties and interfacial behaviour for all the chain lengths and temperatures. Vapour-liquid phase equilibrium is calculated following the standard procedure, equating the pressure and chemical potential in each phase at a given temperature.
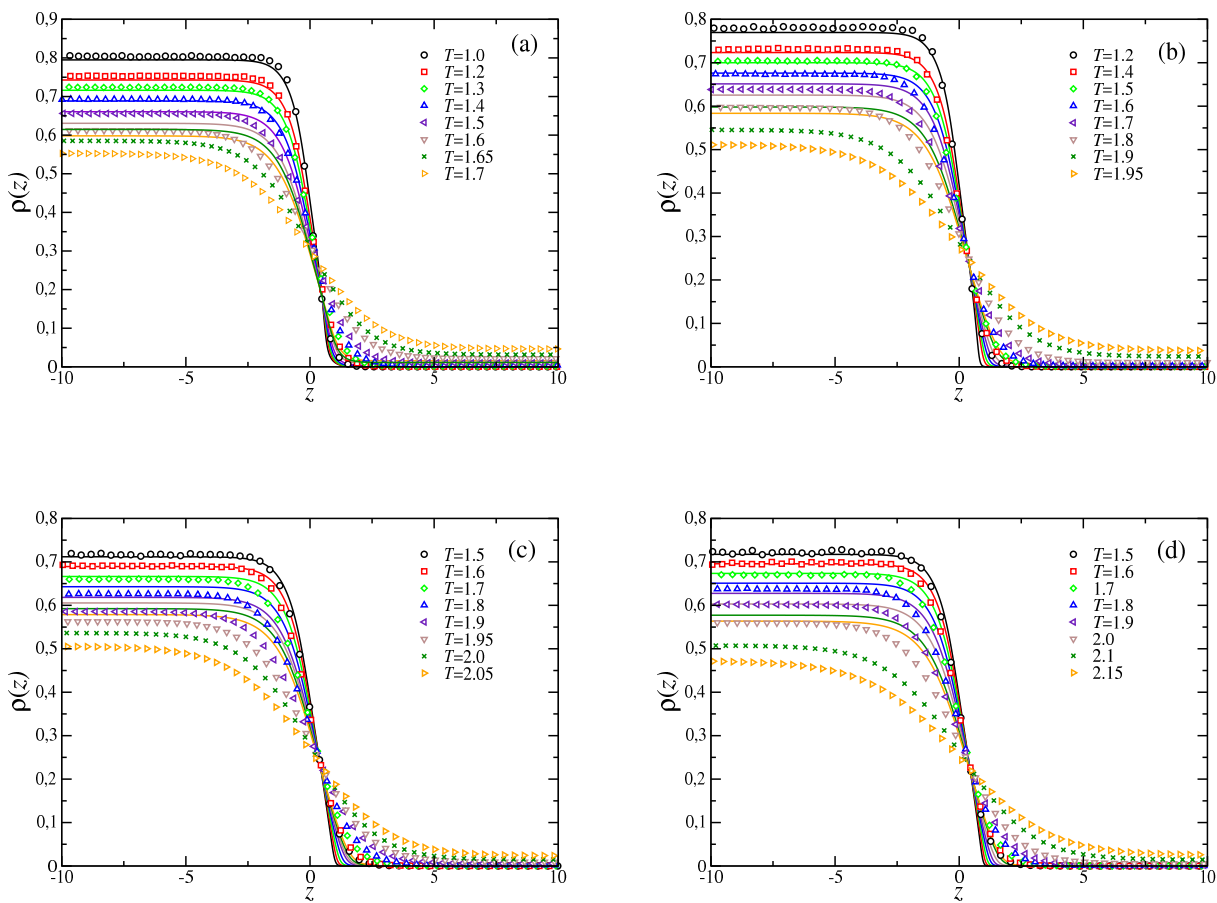
Fig. 1 Equilibrium density profiles across the vapour-liquid interface of fully-flexible TSWC formed from four ($m = 4$), eight ($m = 8$), twelve ($m = 12$), and sixteen ($m = 16$) monomers with potential range $\lambda = 1.5$. From top to bottom (in the liquid region): (a) $m = 4$: $T = 1.0, 1.2.1.3, 1.4, 1.5, 1.6, 1.65$, and 1.7; (b) $m = 8$: $T = 1.2, 1.4.1.5, 1.6, 1.7, 1.8, 1.9$, and 1.95; (c) $m = 12$: $T = 1.5, 1.6.1.7, 1.8, 1.9, 1.95, 2.0$, and 2.05; (c) $m = 16$: $T = 1.5, 1.6.1.7, 1.8, 1.9, 2.0, 2.1$, and 2.15. Symbols correspond to the results obtained from Monte Carlo simulation and curves are the fitting of the simulation data to hyperbolic tangent functions.

Once the bulk properties are determined, the equilibrium density profiles of the inhomogeneous system are obtained solving the Euler-Lagrange equation, which results from the minimisation of the grand potential Ω functional of the system with respect to the density profile, as expressed in Eq. (3). Details relating to the numerical methodology are given in previous work[72,73,82].

In this work, we use the full version of the SAFT-VR DFT, in which correlations in the attractive contribution (see. Eqs. (6) and (7)) are explicitly incorporated in the free energy of the system. In particular, we retain the average correlations at first-order level in the perturbation term described by Eq. (7). A simplified version of the theory, the SAFT-VR MF DFT approach presented previously, could be also used to predict the interfacial properties[72]. It is important to note that both approaches (the full SAFT-VR DFT and the SAFT-VR MF DFT) provide essentially the same density profiles, with slightly different descriptions of the interfacial region. This is because both approaches of the theory provide the same bulk phase behaviour and limiting coexistence densities. However, as it will be seen later, it becomes apparent that correlations should be incorporated to provide the best description of the interfacial tension.

We also determine the equilibrium density profiles $\rho(z)$ from Monte Carlo simulation. We compute $\rho(z)$ from averages of the histogram of densities along the z direction over the production stage. It is important to note that we do not show density profiles of individual segments. Although this information is interesting since provide important information on how molecular chains orientate along the interface, our parametrisation of the theory does not allows to calculate such density profiles, at least in its actual form. Fig. 1 shows the segment density profiles $\rho(z)$ for SW chains formed by four, eight, twelve, and sixteen monomers ($m = 4, 8, 12,$ and 16) at several temperatures in the vapour-liquid coexistence region. For the sake of clarity, we only present one half of the corresponding profiles corresponding to one of the interfaces. Also for convenience, all density profiles have been shifted along z so as to place z_0 at the origin. Our simulation results for the bulk densities and interfacial thickness for SW chains formed from several monomers are collected in Table 1. As can be seen, SAFT-VR DFT approach provides a qualitative prediction of the coexistence of liquid and vapour densities, and reasonable description of the interfacial region, especially at low temperatures for all the chain lengths considered. However, the theory slightly overestimates the liquid densities and underestimates the vapour densities obtained from the direct simulation of the inhomogeneous system with $T/T_c \geq 0.80 - 0.84$. Although this effect is more noticeable as the chain length is increased, it should be taken into account that results from the theory are pure predictions since we have not performed any fitting procedure.

Also notice that we have not taken into account capillary wave broadening of the simulation profiles. Such effects produce a

weak logarithmic increase of the interfacial thickness with lateral system size,[118] but we believe that the relatively small surface areas employed in our simulations do not upset comparison of the simulation results with the mean-field density functional theory calculations.
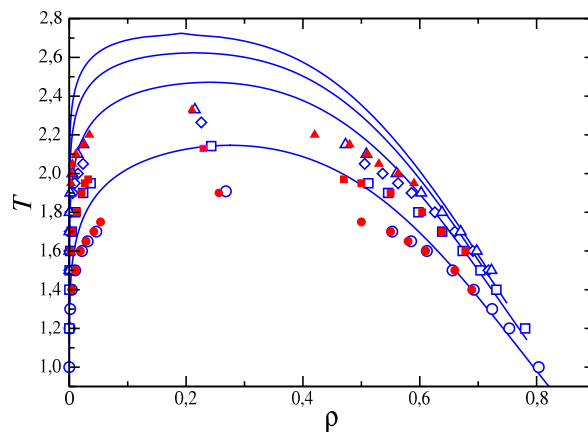
Fig. 2 Vapour-liquid coexistence densities for fully-flexible TSWC with potential range $\lambda = 1.5$. The circles, squares, diamonds, and triangles correspond to the coexistence densities obtained from the analysis of the equilibrium density profiles obtained from Monte Carlo NVT simulations, for chain lengths of $m = 4, 8, 12,$ and 16, respectively. The open symbols correspond to chains studied in this work and filled red symbols to chains taken from the work of Escobedo and de Pablo[42]. The curves represent the predictions obtained from the SAFT-VR formalism and the symbols at the highest temperature for each chain length to the corresponding critical points estimated from Eqs. (10) and (11).

One can compare the vapour-liquid envelope for SW chains of different chain lengths as obtained from the SAFT-VR approach and from the simulation data presented in Table 1. It is also useful to estimate the location of the critical point resulting from our direct Monte Carlo simulations and compare the results with the theoretical predictions as obtained form the SAFT-VR formalism. The estimation of the critical temperature T_c and density ρ_c from Monte Carlo are obtained using the simulation results for the vapour and liquid coexistence densities (Table 1) and the scaling relation for the width of the coexistence curve,

$$\rho_L - \rho_V = A(T - T_c)^\beta , \tag{10}$$

and the law of rectilinear diameters

$$\frac{\rho_L + \rho_V}{2} = B + CT . \tag{11}$$

Here A, B, and C are constants, and β is the corresponding critical exponent. A universal value of $\beta = 0.325$ is assumed here.[119] In

Table 1 Liquid density ρ_L, vapour density ρ_V, vapour pressure P, 10-90 interfacial thickness t, and surface tension γ at different temperatures for systems of fully-flexible TSWC formed from m monomers with potential range $\lambda = 1.5$. All quantities are expressed in the reduced units defined in the Simulation details section. The errors are estimated as explained in the text.

T	ρ_V	ρ_L	P	t	γ
			$m = 4$		
1.0	0.000023(1)	0.8037(14)	0.00000569(24)	0.7373(3)	1.53(8)
1.2	0.000519(5)	0.7530(6)	0.0001276(12)	0.9510(6)	1.00(7)
1.3	0.001636(7)	0.7240(4)	0.0005140(21)	1.091422(24)	0.69(6)
1.4	0.004308(13)	0.6924(3)	0.001407(4)	1.2743(10)	0.49(5)
1.5	0.010027(19)	0.65613(15)	0.003305(6)	1.52862(14)	0.35(3)
1.6	0.02168(4)	0.6120(1)	0.0066(9)	1.9259(6)	0.21(3)
1.65	0.03148(15)	0.58509(19)	0.00965(4)	2.22947(4)	0.19(3)
1.7	0.04619(24)	0.55289(9)	0.01326(8)	2.6934(22)	0.131(22)
			$m = 8$		
1.2	0.000004(4)	0.7804(23)	0.0000005(6)	0.8414(15)	1.10(6)
1.4	0.00013(3)	0.7312(9)	0.000022(5)	1.0536(6)	0.81(5)
1.5	0.00049(3)	0.7039(6)	0.000090(5)	1.1935(3)	0.53(3)
1.6	0.001547(21)	0.6734(4)	0.000298(4)	1.3687(11)	0.52(3)
1.7	0.00419(7)	0.6384(4)	0.000826(13)	1.60476(17)	0.31(3)
1.8	0.0103(1)	0.59758(24)	0.001995(16)	1.9643(8)	0.24(3)
1.9	0.02372(10)	0.54580(20)	0.004308(16)	2.5796(15)	0.108(24)
1.95	0.0365(3)	0.51197(13)	0.00615(4)	3.141(4)	0.069(18)
			$m = 12$		
1.5	0.000039(25)	0.7175(17)	0.000005(3)	1.1073(3)	0.77(5)
1.6	0.00018(3)	0.6910(10)	0.000024(4)	1.2496(10)	0.49(4)
1.7	0.000677(24)	0.6600(5)	0.000094(3)	1.4218(15)	0.38(3)
1.8	0.00211(6)	0.6258(3)	0.000302(8)	1.653(3)	0.29(4)
1.9	0.00576(14)	0.5859(2)	0.000821(18)	1.9890(6)	0.16(3)
1.95	0.00924(14)	0.56273(16)	0.001297(17)	2.2263(5)	0.15(3)
2.0	0.01468(9)	0.53639(23)	0.001996(10)	2.548(3)	0.094(22)
2.05	0.02348(21)	0.50569(19)	0.003005(20)	3.0292(3)	0.084(21)
			$m = 16$		
1.5	0.000003(1)	0.723(3)	0.00000030(9)	1.070(5)	0.80(9)
1.6	0.000023(2)	0.698(3)	0.0000023(2)	1.189(4)	0.52(6)
1.7	0.000129(10)	0.6701(15)	0.0000136(10)	1.340(3)	0.42(4)
1.8	0.000526(9)	0.6380(9)	0.0000581(10)	1.530(3)	0.33(4)
1.9	0.001791(16)	0.6024(5)	0.0002034(17)	1.7872(6)	0.24(4)
2.0	0.00525(6)	0.5602(3)	0.000595(6)	2.16855(4)	0.18(3)
2.1	0.01428(13)	0.50872(17)	0.001519(11)	2.8536(4)	0.12(3)
2.15	0.0242(3)	0.47288(17)	0.002375(20)	3.5094(4)	0.034(24)

Tables 2 and 3 we report the values of the critical densities and temperatures, respectively, as obtained from this procedure for all the systems studied in this work. Note that the values obtained from Eqs. (10) and (11) exhibit a weak system size dependence. A more rigorous analysis would requires the use of a finite-size scaling methodology. However, the main goal of this work is not the exact determination of the critical behaviour of the system. In addition to that, we have also presented the predictions obtained from the SAFT-VR equation. Results from Monte Carlo simulations by Escobedo and de Pablo[42] and from Molecular Dynamics simulations by Chapela and Alejandre[24] also presented for comparison reasons.

The SAFT-VR theoretical predictions overestimate the critical temperatures and critical densities for all the chain lengths considered. As previously mentioned in this section, this is an expected and well-known result since SAFT-VR, as many of the SAFT versions in the literature[89–94], are classical equations of state that do not take into account the fluctuations of the system near the critical point.

The vapour-liquid phase envelopes of TSWC as obtained from the SAFT-VR formalism and the bulk coexistence densities presented in Table 1, calculated from Monte Carlo direct simulation of the interface, are depicted in Fig. 2. Note that densities are again presented in terms of the monomeric segments. The coexistence envelopes exhibit a definite trend with the chain length when represented in terms of the monomeric density. As can be seen in Fig. 2, the phase envelope predicted by the SAFT-VR and calculated from Monte Carlo simulation becomes wider as the chain length is increased, as one would expect. The increase is more significant when the number of monomers is increased from 4 to 8 than when the chain length is further increased. This is consistent with the well-known asymptotic behaviour of the vapour-liquid phase envelope of SW chains expected as $m \to \infty$[120]. Agreement between both results is excellent at low temperatures for all the chain lengths studied. However, as the temperature is increased, agreement between both results is worse. SAFT-VR overestimates the coexistence liquid densities and underestimates the vapour densities for all the chains lengths, especially in the case of $m = 16$. Differences between theory and simulation data are larger as the temperature is higher, for a fixed value of the chain length, as well as the chain length is increased (for a fixed temperature). A similar behaviour is also observed for the critical properties. Differences between theoretical predictions and Monte Carlo simulation data arise mainly due to two reasons. The first one is related with the description of the critical region. Classical equations, included the most sophisticated molecular-based theories such as SAFT, fail to describe the thermodynamic behaviour of fluids close to the critical point. The reason is that these equations are based on the mean-field approximation, which neglects inhomogeneities in the molecular environment. The second one
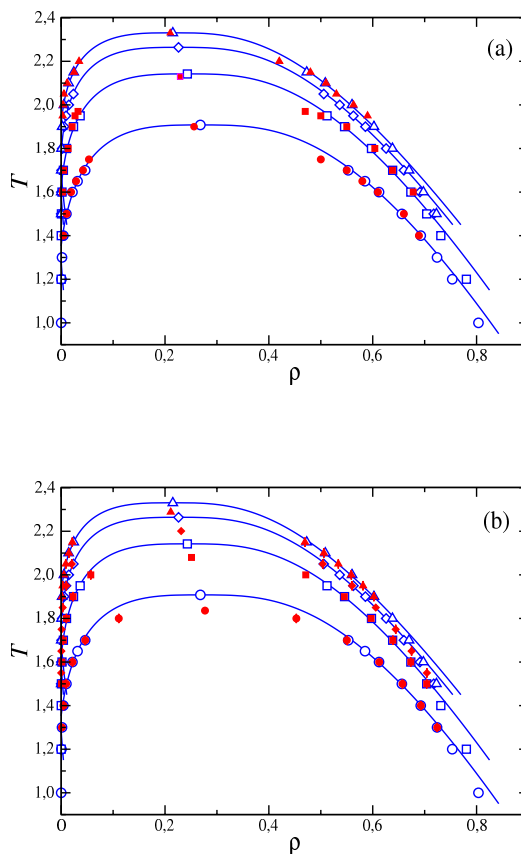
Fig. 3 Vapour-liquid coexistence densities for fully-flexible SW chains with potential range $\lambda = 1.5$. The circles, squares, diamonds, and triangles correspond to the coexistence densities obtained from the analysis of the equilibrium density profiles obtained from Monte Carlo simulations, for chain lengths of $m = 4, 8, 12$, and 16, respectively. The open symbols correspond to the TSWC model studied in this work. The filled red symbols in part (a) are the simulations results obtained by Escobedo and de Pablo[42] for the same molecular model (TSWC) and filled red symbols in part (b) are the simulation data obtained by Chapela and Alejandre[24] for the VSWC model. The curves represent the fits of the simulation data presented in this work to Eqs. (10) and (11), and the symbols at the highest temperature for each chain length to the corresponding critical points estimated from the previous equations.

Table 2 Critical density obtained from the SAFT-VR equation of state† and from the analysis of the coexistence densities using Eqs. (10) and (11). Results correspond to the TSWC model studied by Escobedo and de Pablo§, to the TSWC model analysed in this work‡, and to the VSWC model studied by Chapela and Alejandre¶. dev($\rho_c^§, \rho_c^‡$) and dev($\rho_c^§, \rho_c^¶$) are the relative deviations between the indicated critical densities. All results correspond to fully-flexible SW chains with potential range $\lambda = 1.5$ and are expressed in the reduced units defined in Section 2.

m	$\rho_c^†$	$\rho_c^§$	$\rho_c^‡$	dev($\rho_c^§, \rho_c^‡$)	$\rho_c^¶$	dev($\rho_c^§, \rho_c^¶$)
4	0.2754	0.2559	0.268(3)	4.73%	0.277(1)	8.25%
8	0.2405	0.2291	0.243(5)	6.07%	0.251(1)	9.56%
12	0.2137	-	0.226(6)	-	0.231(3)	-
16	0.1915	0.2101	0.215(10)	2.33%	0.218(3)	3.76%

arises from the linear approximation in the Wertheim's first-order Thermodynamic Perturbation Theory or TPT1. One of the weakest points of Wertheim's theory (and SAFT) is that it does not correctly account for the intramolecular interactions of chains; hence, it predicts a nonphysical behaviour in the same properties at low density limit [121,122]. This is not a defect of the theory, but a consequence of the first-order approximation. At this level of description, the many-body distribution functions are approximated as a product pair distribution functions. In other words, at low densities only consecutive monomers of the chains are correlated. This problem does not arise at high densities since the chain-chain interpenetrations become more important and the structure of the fluids is dominated by the repulsive forces.

We compare the coexisting vapour and liquid densities obtained from direct coexistence of the inhomogeneous systems (see Table 1) with the results determined by Escobedo and de Pablo. Fig. 3a shows the vapour-liquid phase envelopes of TSWC obtained in this work and those corresponding to Escobedo and de Pablo. As can be seen, simulation results obtained from direct simulation of the vapour-liquid interface and from Gibbs ensemble Monte Carlo simulation are nearly identical. Small differences are seen at high temperatures for a given chain length and close to critical point, especially in the case $m = 4$. This discrepancy could be attributed to finite-size scaling effects near the critical point because the simulation boxes used in both works are different.

We also compare our results for the phase equilibrium with that of VSWC obtained by Chapela and Alejandre using Molecular Dynamics simulations (Fig. 3b). In this case, both simulation results are obtained from direct simulation of the vapour-liquid interface. Differences between both results can be observed at temperatures close to the critical temperature of each chain length. It is important to remember that in the case of the VSWC, the intramolecular distance between consecutive SW monomers is not equal to the diameter of the segments but 0.97 times that diameter.

We have summarised the simulation data corresponding to the critical temperatures and densities of the TSWC and VSWC models in Tables 2 and 3. We include results obtained in this work, as well as simulation data obtained by Escobedo and de Pablo and Chapela and Alejandre for both models. As can be seen, differences between critical temperatures and densities for all the
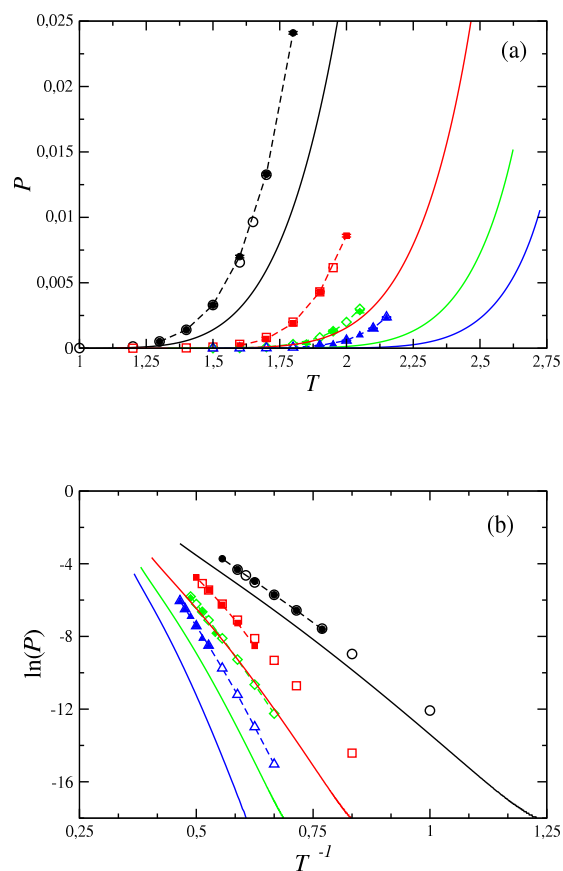
Fig. 4 Vapour pressure curves (a) and Clausius-Clapeyron plot (b) for fully-flexible SW chains with potential range $\lambda = 1.5$. The black circles, red squares, green diamonds, and blue triangles correspond to the vapour pressure for chain lengths of $m = 4$, $m = 8$, $m = 12$, and $m = 16$, respectively. The open symbols correspond to simulation results obtained from the thermodynamic integration analysis of Eq. (9) explained in Section 3 of the TSWC model and filled symbols are the simulation results obtained by Chapela and Alejandre [24] (VSWC model). The continuous curves are the predictions from the SAFT-VR formalism. The dashed curves are included as a guide to the eyes.

Table 3 Critical temperature obtained from the SAFT-VR equation of state[†] and from the analysis of the coexistence densities using Eqs. (10) and (11). Results correspond to the TSWC model studied by Escobedo and de Pablo[§], to the TSWC model analysed in this work[‡], and to the VSWC model studied by Chapela and Alejandre[¶]. dev($T_c^§, T_c^‡$) and dev($T_c^§, T_c^¶$) are the relative deviations between the indicated critical densities. All results correspond to fully-flexible SW chains with potential range $\lambda = 1.5$ and are expressed in the reduced units defined in Section 2.

m	$T_c^†$	$T_c^§$	$T_c^‡$	dev($T_c^§, T_c^‡$)	$T_c^¶$	dev($T_c^§, T_c^¶$)
4	2.1499	1.90	1.908(3)	0.42%	1.836(1)	3.37%
8	2.4719	2.13	2.142(5)	0.56%	2.080(1)	2.35%
12	2.6239	-	2.264(6)	-	2.201(5)	-
16	2.7246	2.33	2.33(1)	0%	2.284(1)	1.97%

chain lengths are noticeable. In particular, the results obtained in this work are in better agreement with simulation data presented by Escobedo and de Pablo than with those of Chapela and Alejandre. It is also interesting to note that differences between critical densities and temperatures decrease as the chain length is increased, especially in the the case of critical densities. Our results are in agreement with previous results obtained by Hu *et al.*[43], which show that the binodals of VSWC are slightly different than those corresponding to TSWC. Although this could be due to finite-size scaling effects near the critical point, it also possible, as it will be clear later, that the both models (TSWC and VSWC) are not indeed completely equivalent.

We also consider the behaviour of the vapour pressure of SW chains as a function of temperature. In particular, we analyse the results obtained from simulations using the procedure explained in section 3, as well as from the SAFT-VR approach. Fig. 3 shows the theoretical predictions from the SAFT-VR approach and simulation results obtained for the vapour pressure of the chains studied. The simulation results for the vapour pressure are also presented in Table 1. The SAFT-VR approach, as in the case of the vapour-liquid coexistence envelopes, provides a qualitative description of the vapour pressure of chains formed from several SW monomeric units. Unfortunately, SAFT-VR overestimates the vapour pressure at all temperatures, for a fixed value of the chain length. Differences increase as the temperature approaches to the critical temperature for a particular value of the chain length. In addition to that, at a given temperature, the theoretical predictions become worse as the chain length is increased. This behaviour is in agreement with conclusions obtained from the analysis of the vapour-liquid phase envelope.

Fig. 3 also includes the results corresponding to the simulation data obtained by Chapela and Alejandre. They have obtained the vapour pressure from the normal component of the pressure tensor following the mechanical virial route. As can be seen, agreement between the results of Chapela and Alejandre obtained from the virial route and the results obtained in this work using the thermodynamic integration explained above is remarkable for all the chain lengths and temperatures in the whole liquid-vapour coexistence range, including the region near the critical point. It is important to mention that statistical uncertainties obtained in this work are smaller that those corresponding to the simulations
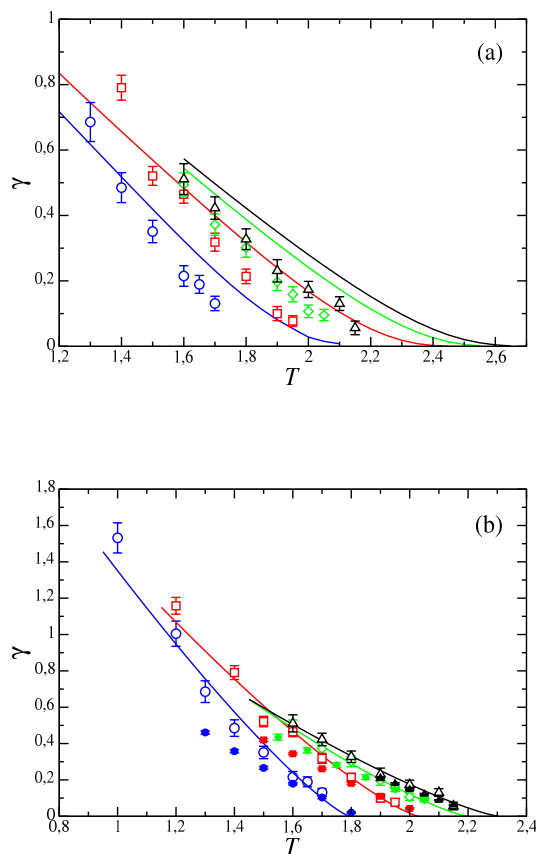
Fig. 5 Vapour-liquid surface tension for fully-flexible SW chains with potential range $\lambda = 1.5$. The black circles, red squares, green diamonds, and blue triangles correspond to the vapour pressure for chain lengths of $m = 4$, $m = 8$, $m = 12$, and $m = 16$, respectively. In part (a), the continuous curves correspond to the predictions obtained from the SAFT-VR DFT formalism and the open symbols correspond to chains studied in this work (TSWC). In part (b), the continuous curves represent the fits of the simulation data obtained in this work to the scaling relationship of the surface tension near the critical point with Eq. (12), the open symbols are the simulation data obtained in this work for TSWC model, and the filled symbols are the simulation data of Chapela and Alejandre[24] for the VSWC model.

of Chapela and Alejandre (see Table 1 of this work and Tables IV, V, VII, and VIII of the manuscript of Chapela and Alejandre [24]). In particular, errors here are one or two orders of magnitude lower than those corresponding to the work of Chapela and Alejandre. This is an expected results since the method for calculating the vapour pressure is very accurate and robust, in comparison with that used by Chapela and Alejandre, which is based on the average of the normal component of the pressure tensor along the vapour-liquid interface.

Finally, the vapour-liquid surface tension data obtained from molecular simulation using the WIM approach for TSWC with a range $\lambda = 1.5$ are compared with the theoretical predictions determined from the SAFT-VR DFT formalism in Fig. 5a. As can be seen, at any given temperature, the interfacial tension is larger for longer chains. Once again, this is consistent with the large cohesive energy in systems consisting of long chains. An essentially linear behaviour is found for the range of temperatures considered here, with a slight curvature close to the critical point for each system. The effect of chain length on the slope of the surface tension curves is remarkable. At a given temperature, this slope becomes less negative as m is increased, a trend which is also exhibited by the first members of the n-alkane series.[73] The same qualitative behaviour has been previously found by Bryk and collaborators.[123] One should keep in mind, however, that a TSWC model is not the most appropriate representation of real n-alkanes.

The theoretical predictions shown in Fig. 5a overestimate the vapour-liquid surface tension in all cases, especially close to the critical point corresponding to each chain length. However, at low temperatures and particularly for the cases $m = 4$ and $m = 8$, the SAFT-VR DFT formalism underestimates the surface tension values obtained from Monte Carlo simulation. This behaviour has been observed previously in other model and real systems[72,73]. It is important to recall here that the SAFT-VR DFT approach is a classic formalism that neglects the long-range fluctuations associated with the critical phenomena. Is is possible to use a more sophisticated version of SAFT including the long-range corrections due to the critical points, as proposed several years ago by Gross[74]. This approach, which is strictly more rigorous, implies unfortunately an increasing complexity in computational calculations.

The computed values of the surface tension obtained by computer simulation allow us to obtain an independent estimate of the critical temperature for each chain length from the scaling relation

$$\gamma = \gamma_0 \left(1 - T/T_c\right)^{\mu} , \qquad (12)$$

where γ is the surface tension at temperature T, γ_0 is the "zero-temperature" surface tension, μ is the corresponding critical exponent, and T_c is the critical temperature. Here, we fix μ to the universal value of $\mu = 1.258$ as obtained from renormalization-group theory.[119] Our estimates for the critical temperatures are collected in Table 3. The overall agreement between these values and those obtained from an analysis of the coexistence densities is satisfactory.

Finally, it is also interesting to compare our computed values of the surface tension with those reported by Chapela and Alejandre for the VSWC model with potential range $\lambda = 1.5$. Although the models are similar, as we have discussed previously in this work, the model used by Chapela and Alejandre has a slightly smaller intramolecular length between the spherical segments forming the SW chains. Fig. 5b shows the comparison of the the surface tension, as a function of temperature, as obtained in this work and by Chapela and Alejandre. We have also included the scaling relation given by Eq. (12) using the simulation data presented in Table 1. Results obtained for the VSWC indicate that surface tension is lower than surface tension of the tangent fully-flexible chain model at low temperatures. Discrepancies between both results are larger for the shortest chains ($m = 8$ and especially $m = 4$). As the temperature is increased, at intermediate and high temperatures, close to the critical temperature, results from Chapela and Alejandre and those obtained in this work become nearly identical. Although the molecular models seem to be very similar, we attribute the discrepancies between both results due to the differences in the bond length and flexibility.

5 Conclusions

We have determined the interfacial properties of the vapour-liquid interface of fully-flexible chains formed from tangentially bonded SW monomers (TSCW model) with potential range $\lambda = 1.5$ using the Statistical Associating Fluid Theory for Variable Range (SAFT-VR) density functional theory (DFT). Chains formed by four, eight, twelve, and sixteen monomers are considered. Both intermolecular and intramolecular segment-segment interactions are taken into account explicitly in this work. We have also used Monte Carlo NVT simulation of the inhomogeneous system containing two vapour-liquid interfaces. The surface tension is evaluated using the wandering interface method (WIM). We have examined the density profiles and surface tension in terms of the temperature and the number of monomers forming the chains. In addition, we have also calculated the coexistence phase envelope and the vapour pressure, including the location of the critical point from an analysis of the density profiles and the surface tension.

The effect of the chain length on the density profiles, coexistence densities, vapour pressures, critical temperature and density, and surface tension has been investigated. The vapour-liquid interface is seen to sharpen with increasing chain length corresponding to an increase in the width of the coexistence phase envelope, and an accompanying increase in the surface tension. The

coexistence phase envelope, the interfacial thickness and the surface tension are seen to exhibit an asymptotic limiting behaviour as the chains get longer. The theory is able to predict the general trends exhibited by the system, although agreement with simulation data for the same molecular model is only qualitative.

Finally, we have also compared the results obtained in our simulations with simulation data obtained independently by Escobedo and de Pablo for the same molecular model (TSWC) and by Chapela and Alejandre for the VSWC model, including vapourliquid coexistence densities, vapour pressures, and surface tension. In the case of the coexistence densities and vapour pressures, agreement between our simulation results and those taken from the literature for both models (TSWC and VSWC) are excellent in all cases. Slightly differences at high temperatures, close to the critical point, can be observed in coexistence densities. This is probably due to the difference in the molecular models. Whereas in the TSWC model we use here the segments forming the fully flexible chains are strictly tangent, in the VSWC model the intramolecular distance between consecutive segments is 0.97 (and not 1.0) in reduced units.

Acknowledgements

Appendix: Excess free energy contributions

The reference contribution of the SAFT-VR free energy functional used in this work incorporates all the contributions to the free energy due to "short-range" interactions such as the ideal term, the repulsive hard-sphere term, and the chain term,

$$F^{\text{ref}}[\rho(\mathbf{r})] = F^{\text{ideal}}[\rho(\mathbf{r})] + F^{\text{hs}}[\rho(\mathbf{r})] + F^{\text{chain}}[\rho(\mathbf{r})] + F_2[\rho(\mathbf{r})] \quad (13)$$

For convenience, it is useful to examine the functional in terms of reduced free energy density $f[\rho(\mathbf{r})] \equiv F[\rho(\mathbf{r})]/Vk_BT \equiv \rho(\mathbf{r})a[\rho(\mathbf{r})]$.

The reduced ideal Helmholtz free energy of an inhomogeneous system of non-spherical particles can be written as,

$$F^{\text{ideal}}[\rho(\mathbf{r})] = k_BT \int d\mathbf{r} \, f^{\text{ideal}}(\rho(\mathbf{r})) = k_BT \int d\mathbf{r} \, \rho(\mathbf{r}) a^{\text{ideal}}(\rho(\mathbf{r})) \quad (14)$$

where the form of the density dependence of $a^{\text{ideal}}(\rho(\mathbf{r}))$ is given by,

$$a^{\text{ideal}}(\rho) \equiv \frac{F^{\text{ideal}}}{Nk_BT} = \ln(\rho\Lambda^3) - 1 \quad (15)$$

Here $\rho = N/V$ is the number density of chain molecules, and Λ is a thermal de Broglie wavelength which contains the translational and rotational contributions to the partition function of the ideal chain.

The hard-sphere interaction is short ranged and is usually treated locally in a perturbative DFT treatment of the vapourliquid interface. In our SAFT-VR DFT, the hard-sphere LDA free energy functional is given by,

$$F^{\text{hs}}[\rho(\mathbf{r})] = k_BT \int d\mathbf{r} \, f^{\text{hs}}(\rho(\mathbf{r})) = k_BT \int d\mathbf{r} \, \rho(\mathbf{r}) m a^{\text{hs}}(\rho(\mathbf{r})) \quad (16)$$

The expression for $a^{\text{hs}}(\rho(\mathbf{r}))$ is written as a function of the packing fraction profile $\eta(\mathbf{r}) = (m\pi\sigma^3/6)\rho(\mathbf{r})$,

$$a^{\text{hs}}(\rho) \equiv \frac{F^{\text{hs}}}{N_sk_BT} = \frac{4\eta - 3\eta^2}{(1-\eta)^2} \quad (17)$$

Here $\eta = \pi\sigma^3\rho_s/6 = \pi\sigma^3 m\rho/6$ is the usual packing fraction, and $\rho_s = N_s/V$ is the number density of segments.

The contribution to the reference free energy functional for the formation of a chain of m square-well segments is written at the LDA level as,

$$F^{\text{chain}}[\rho(\mathbf{r})] = k_BT \int d\mathbf{r} \, f^{\text{chain}}(\rho(\mathbf{r})) = k_BT \int d\mathbf{r} \, \rho(\mathbf{r}) a^{\text{chain}}(\rho(\mathbf{r})) \quad (18)$$

where $a^{\text{chain}}(\rho(\mathbf{r}))$ is the function of density given by,

$$a^{\text{chain}}(\rho) \equiv \frac{F^{\text{chain}}}{Nk_BT} = -(m-1)\ln y^{\text{sw}}(\sigma;\rho) \quad (19)$$

$y^{\text{sw}}(\sigma;\rho) = \exp(-\varepsilon/k_BT)g^{\text{sw}}(\sigma;\rho)$ is the contact value of the background (cavity) pair correlation function for a system of squarewell monomers. In the SAFT-VR approach the contact value of the pair radial distribution function $g^{\text{sw}}(\sigma;\rho)$ is obtained from a firstorder high-temperature expansion about a hard-sphere reference system,

$$g^{\text{sw}}(\sigma;\rho) = g^{\text{hs}}(\sigma;\rho) + \frac{1}{4}\left[\frac{\partial a_1}{\partial \eta} - \frac{\lambda}{3\eta}\frac{\partial a_1}{\partial \lambda}\right] \quad (20)$$

The contact value $g^{\text{hs}}(\sigma;\rho)$ of the correlation function for the hard-sphere system is represented by the Carnahan and Starling expression,

$$g^{\text{hs}}(\sigma;\rho) = \frac{1 - \eta/2}{(1-\eta)^3} \quad (21)$$

The mean-attractive dispersive energy a_1 is usually write in terms of a contact value of the system at an effective density ρ_{eff} (or

effective packing fraction, $\eta_{\text{eff}} = \pi\sigma^3 m\rho_{\text{eff}}/6$),

$$a_1 = a_1^{\text{vdW}} g^{\text{hs}}(\sigma;\rho_{\text{eff}}) \tag{22}$$

The pre-factor a_1^{vdW} is the van der Waals dispersive free energy is given by,

$$a_1^{\text{vdW}} = -\frac{2\pi\rho_s}{k_B T}\sigma^3\varepsilon(\lambda^3 - 1) \tag{23}$$

The contact value of the pair distribution for the hard-sphere fluid at the effective density ρ_{eff} (or correspondingly at the effective packing fraction η_{eff}) is given by,

$$g^{\text{hs}}(\sigma;\rho_{\text{eff}}) = \frac{1 - \eta_{\text{eff}}/2}{(1 - \eta_{\text{eff}})^3} \tag{24}$$

The dependence of η_{eff} on the actual packing fraction η and the range of the square-well potential λ is obtained by using a very accurate description of the structure of the hard-sphere reference system with the following parameterisation,

$$\eta_{\text{eff}} = c_1\eta + c_2\eta^2 + c_3\eta^3 \tag{25}$$

where the coefficients c_n are obtained from the matrix,

$$\begin{pmatrix} c_1 \\ c_2 \\ c_3 \end{pmatrix} = \begin{pmatrix} 2.25855 & -1.05349 & 0.249434 \\ -0.69270 & 1.40049 & -0.827739 \\ 10.1576 & -15.0427 & 5.30827 \end{pmatrix} \begin{pmatrix} 1 \\ \lambda \\ \lambda^2 \end{pmatrix} \tag{26}$$

Finally, the contribution to the reference term associated to the high-temperature perturbation expansion of the second order is also treated locally,

$$F_2[\rho(\mathbf{r})] = k_B T \int d\mathbf{r}\, f_2(\rho(\mathbf{r})) = k_B T \int d\mathbf{r}\, \rho(\mathbf{r})\, m\, a_2(\rho(\mathbf{r})), \tag{27}$$

where $a_2(\rho(\mathbf{r}))$ is given by,

$$a_2(\rho) \equiv \frac{A_2}{N_s k_B T} = \frac{1}{2}\frac{\varepsilon}{k_B T} K^{\text{hs}}\eta a_1'. \tag{28}$$

This fluctuation term is expressed in terms of the local compressibility approximation (LCA) of Barker and Henderson. In this relation $a_1'(\rho) = \partial a_1/\partial\eta$ represents the density derivative of the mean-attractive energy, and K^{hs} is the Percus-Yevick expression for the hard-sphere compressibility factor given by,

$$K^{\text{hs}} = \frac{(1-\eta)^4}{1 + 4\eta + 4\eta^2}. \tag{29}$$

References

1 R. Evans, *Density Functionals in the Theory of Nonuniform Fluids. In Fundamentals of Inhomogeneous Fluids*, Dekker, New York, 1992.

2 V. K. Shen, R. D. Mountain and J. R. Errington, *J. Phys. Chem. B*, 2007, **111**, 6198–6207.

3 V. K. Shen and J. R. Errington, *J. Chem. Phys.*, 2006, **124**, 024721/1–9.

4 V. K. Shen and J. R. Errington, *J. Chem. Phys.*, 2005, **122**, 064508/1–17.

5 G. J. Gloor, G. Jackson, F. J. Blas and E. de Miguel, *J. Chem. Phys.*, 2005, **123**, 134703/1–19.

6 A. Trokhymchuk and J. Alejandre, *J. Chem. Phys.*, 1999, **111**, 8510–8523.

7 J. Janeček, *J. Phys. Chem. B*, 2006, **110**, 6264–6269.

8 J. R. Errington and D. A. Kofke, *J. Chem. Phys.*, 2007, **127**, 174709/1–12.

9 L. G. MacDowell and P. Bryk, *Phys. Rev. E*, 2007, **75**, 061609/1–13.

10 E. Día-Herrera, J. Alejandre, G. Ramírez-Santiago and F. Forstmann, *J. Chem. Phys.*, 1999, **110**, 8084/1–8.

11 E. Díaz-Herrera, G. Ramírez-Santiago and J. A. Moreno-Razo, *Phys. Rev. E*, 2003, **68**, 061204/1–8.

12 E. Díaz-Herrera, J. A. Moreno-Razo and G. Ramírez-Santiago, *Phys. Rev. E*, 2004, **70**, 051601/1–8.

13 E. Díaz-Herrera, G. Ramírez-Santiago and J. A. Moreno-Razo, *J. Chem. Phys.*, 2005, **123**, 184507/1–9.

14 G. Galliero, M. M. P. neiro, B. Mendiboure, C. Miqueu, T. Lafitte and D. Bessieres, *J. Chem. Phys.*, 2009, **130**, 104704/1–10.

15 P. Orea, Y. Reyes-Mercado and Y. Duda, *Phys. Lett. A*, 2008, **372**, 7024–7027.

16 Y. Duda, A. Romero-Martínez and P. Orea, *J. Chem. Phys.*, 2007, **126**, 224510/1–4.

17 J. K. Singh and S. K. Kwak, *J. Chem. Phys.*, 2007, **126**, 024702/1–8.

18 G. Odriozola, M. Bárcenas and P. Orea, *J. Chem. Phys.*, 2011, **134**, 154702/1–5.

19 M. González-Melchor, G. Hernández-Cocoletzi, J. López-Lemus, A. Ortega-Rodríguez and P. Orea, *J. Chem. Phys.*, 2012, **136**, 154702/1–6.

20 U. F. Galicia-Pimentel, J. López-Lemus and P. Orea, *Fluid Phase Equil.*, 2008, **265**, 205–208.

21 E. de Miguel, *J. Phys. Chem. B*, 2008, **112**, 4674–4679.

22 P. Orea, Y. Dud and J. Alejandre, *J. Chem. Phys.*, 2003, **118**, 5635–5639.

23 J. K. Singh, D. A. Kofke and J. R. Errington, *J. Chem. Phys.*, 2003, **119**, 3405–3412.

24 G. A. Chapela and J. Alejandre, *J. Chem. Phys.*, 2011, **135**, 084126/1–11.

25 G. A. Chapela, E. Día-Herrera, J. C. Armas-Pérez and

J. Quintana-H, *J. Chem. Phys.*, 2013, **138**, 224509/1–9.

26 G. Jimenez-Serratos, C. Vega and A. Gil-Villegas, *J. Chem. Phys.*, 2011, **137**, 204104/1–12.

27 J. K. Singh, G. Sarma and S. K. Kwak, *J. Chem. Phys.*, 2008, **128**, 044708/1–8.

28 H. Peng, A. V. Nguyen and G. Birkett, *Mol. Simul.*, 2013, **39**, 129–136.

29 M. Müller and L. G. MacDowell, *Macromolecules*, 2000, **33**, 3902–3923.

30 A. I. Milchev and A. A. Milchev, *Europhys. Lett*, 2001, **56**, 695–701.

31 F. Varnik, J. Baschnagel and K. Binder, *J. Chem. Phys.*, 2000, **113**, 4444–4453.

32 P. Virnau, M. Müller, L. G. MacDowell and K. Binder, *J. Chem. Phys.*, 2004, **121**, 2169–2179.

33 B. M. Mognetti, L. Yelash, P. Virnau, W. Paul, K. Binder, M. Müller and L. G. MacDowell, *J. Chem. Phys.*, 2008, **128**, 104501/1–13.

34 J. P. Hansen and I. R. McDonald, *Theory of Simple Liquids, 3rd Edition*, Academic Press, London, 2006.

35 J. Wu and Z. Li, *Annu. Rev. Phys. Chem.*, 2007, **58**, 85–112.

36 J. Wu, *AIChE Journal.*, 2006, **52**, 1169–1193.

37 C. P. Emborsky, Z. Feng, K. R. Cox and W. G. Chapman, *Fluid Phase Equil.*, 2011, **306**, 15–30.

38 J. Landers, G. Y. Gor and A. V. Neimark, *Colloids Surf. A*, 2013, **437**, 3–32.

39 H. T. Davis, *Statistical Mechanics of Phases, Interfaces, and Thin Films*, VCH, Weinheim, 1996.

40 J. S. Rowlinson, *J. Stat. Phys.*, 1979, **20**, 197–244.

41 J. W. Cahn and J. E. Hilliard, *J. Chem. Phys.*, 1958, **28**, 258–267.

42 F. Escobedo and J. J. de Pablo, *Mol. Phys.*, 1996, **87**, 347–366.

43 L. Hu, H. Rangwalla, J. Cui and J. R. Elliot, *J. Chem. Phys.*, 1999, **111**, 1293–1301.

44 D. B. Macleod, *Trans. Faraday Soc.*, 1923, **19**, 38–41.

45 E. A. Guggenheim, *J. Chem. Phys.*, 1945, **13**, 253–261.

46 P. W. W. Cornelisse, C. J. Peters and J. de Swaan Arons, *Fluid Phase Equil.*, 1993, **82**, 119–129.

47 P. W. W. Cornelisse, C. J. Peters and J. de Swaan Arons, *Fluid Phase Equil.*, 1996, **117**, 312–319.

48 H. Kahl and S. Enders, *Phys. Chem. Chem. Phys.*, 2002, **4**, 931–936.

49 L. E. Urlic, L. J. Florusse, E. J. M. Straver, S. Desgrange and C. J. Peters, *Transport Porous Media*, 2003, **52**, 141–157.

50 C. Miqueu, B. Mendiboure, A. Graciaa and J. Lachaise, *Fluid Phase Equil.*, 2004, **218**, 189–203.

51 C. Miqueu, B. Mendiboure, A. Graciaa and J. Lachaise, *Ind.*

52 A. Mejía, H. Segura, L. F. Vega and J. Wisniak, *Fluid Phase Equil.*, 2005, **227**, 225–238.

53 A. Mejía, H. Segura, J. Wisniak and I. Polishuk, *J. Phase Equilibr. Diffusion*, 2005, **26**, 215–224.

54 C. Miqueu, B. Mendiboure, A. Graciaa and J. Lachaise, *Fuel*, 2008, **87**, 612–621.

55 X. S. Li, J. M. Liu and D. Fu, *Ind. Eng. Chem. Res.*, 2008, **47**, 8911–8917.

56 M. B. Oliveira, J. M. Marrucho and J. A. P. C. ansd A. J. Queimada, *Fluid Phase Equil.*, 2008, **267**, 83–91.

57 D. Fu and Y. Wei, *Ind. Eng. Chem. Res.*, 2008, **47**, 4490–4495.

58 D. Fu, H. J. Jian and B. S. Wang, *Fluid Phase Equil.*, 2009, **279**, 136–140.

59 E. A. Müller and A. Mejía, *Fluid Phase Equil.*, 2009, **282**, 68–81.

60 T. Lafitte, B. Mendiboure, M. M. P. neiro, D. Bessieres and C. Miqueu, *J. Phys. Chem. B*, 2010, **114**, 11110–11116.

61 O. G. N. no Amèzquita, S. Enders, P. T. Jaeger and R. Eggers, *J. Supercrit. Fluids*, 2010, **55**, 724–734.

62 C. Miqueu, J. M. Míguez, M. M. Piñeiro, T. Lafitte and B. Mendiboure, *J. Phys. Chem. B*, 2011, **115**, 9618–9625.

63 Y. Rosenfeld, *Phys. Rev. Lett.*, 1989, **63**, 980–983.

64 R. Roth, R. Evans, A. Lang and G. Kahl, *J. Phys. Condens. Matter*, 2002, **14**, 12063–12078.

65 Y. X. Yu and J. Z. Wu, *J. Chem. Phys.*, 2002, **117**, 2368–2376.

66 S. Tripathi and W. G. Chapman, *J. Chem. Phys.*, 2005, **122**, 094506/1–11.

67 S. Tripathi, A. Dominik and W. G. Chapman, *Ind. Eng. Chem. Res.*, 2006, **45**, 6785–6792.

68 S. Jain, A. Dominik and W. G. Chapman, *J. Chem. Phys.*, 2007, **127**, 244904/1–12.

69 P. Bryk, K. Bucior and S. Sokolowski, *J. Phys. Chem. C*, 2007, **111**, 15523–15532.

70 J. Winkelmann, *J. Phys. Condens. Matter*, 2001, **13**, 4739–4768.

71 H. Kahl, M. Mecke and J. Winkelmann, *Fluid Phase Equil.*, 2005, **228-229**, 293–302.

72 G. J. Gloor, G. Jackson, F. J. Blas, E. Martín del Río and E. de Miguel, *J. Chem. Phys.*, 2004, **121**, 12740–12759.

73 G. J. Gloor, G. Jackson, F. J. Blas, E. M. del Río and E. de Miguel, *J. Phys. Chem. C*, 2007, **111**, 15513–15522.

74 J. Gross, *J. Chem. Phys.*, 2009, **131**, 204705/1–12.

75 X. H. Tang and J. Gross, *J. Supercrit. Fluids*, 2010, **55**, 735–742.

76 S. Toxvaerd, *J. Chem. Phys.*, 1971, **55**, 3116–3120.

77 S. Toxvaerd, *Mol. Phys.*, 1973, **26**, 91–99.

78 S. Toxvaerd, *J. Chem. Phys.*, 1976, **64**, 2863–2867.

79 F. J. Blas, E. Martín del Río, E. de Miguel and G. Jackson, *Mol. Phys.*, 2001, **99**, 1851–1865.

80 G. J. Gloor, F. J. Blas, E. M. del Río, E. de Miguel and G. Jackson, *Fluid Phase Equil.*, 2002, **194-197**, 521–530.

81 F. Llovell, A. Galindo, G. Jackson and F. J. Blas, *J. Chem. Phys.*, 2010, **133**, 024704/1–19.

82 F. Llovell, N. MacDowell, A. Galindo, G. Jackson and F. J. Blas, *Fluid Phase Equil.*, 2012, **336**, 137–150.

83 A. Gil-Villegas, A. Galindo, P. J. Whitehead, S. J. Mills, G. Jackson and A. N. Burgess, *J. Chem. Phys.*, 1997, **106**, 4168–4186.

84 A. Galindo, L. A. Davies, A. Gil-Villegas and G. Jackson, *Mol. Phys.*, 1998, **93**, 241–252.

85 G. Jackson, W. G. Chapman and K. E. Gubbins, *Mol. Phys.*, 1988, **65**, 1–31.

86 W. G. Chapman, G. Jackson and K. E. Gubbins, *Mol. Phys.*, 1988, **65**, 1057–1079.

87 G. Jackson and K. E. Gubbins, *Pure Applied Chemistry*, 1989, **61**, 1021–1026.

88 W. G. Chapman, K. E. Gubbins, G. Jackson and M. Radosz, *Fluid Phase Equil.*, 1989, **52**, 31–38.

89 E. A. Müller and K. E. Gubbins, *Ind. Eng. Chem. Res.*, 1995, **34**, 3662–3673.

90 P. Paricaud, A. Galindo and G. Jackson, *Fluid Phase Equil.*, 2002, **194–197**, 87–96.

91 I. G. Economou, *Ind. Eng. Chem. Res.*, 2002, **41**, 953–962.

92 S. P. Tan, H. Adidharma and M. Radosz, *Ind. Eng. Chem. Res.*, 2008, **47**, 8063–8082.

93 C. McCabe and A. Galindo, *Applied Thermodynamics of Fluids*, Royal Society of Chemistry, London, 2010, ch. 8.

94 E. A. Müller and G. Jackson, *Annu. Rev. Chem. Biomol. Eng.*, 2014, **5**, 405–427.

95 M. S. Wertheim, *J. Stat. Phys.*, 1984, **35**, 19–34.

96 M. S. Wertheim, *J. Stat. Phys.*, 1984, **35**, 35–47.

97 M. S. Wertheim, *J. Stat. Phys.*, 1986, **42**, 459–476.

98 M. S. Wertheim, *J. Stat. Phys.*, 1986, **42**, 477–492.

99 M. S. Wertheim, *J. Chem. Phys.*, 1986, **85**, 2929–2936.

100 M. S. Wertheim, *J. Chem. Phys.*, 1987, **87**, 7323–7331.

101 P. Bryk and L. G. MacDowell, *J. Chem. Phys.*, 2011, **135**, 204901/1–9.

102 H. Kahl and J. Winkelmann, *Fluid Phase Equil.*, 2008, **270**, 50–61.

103 S. Jain and W. G. Chapman, *Mol. Phys.*, 2009, **107**, 1–17.

104 C. Malheiro, B. Mendiboure, F. Plantier, F. J. Blas and C. Miqueu, *J. Chem. Phys.*, 2014, **140**, 134707/1–9.

105 S. Figueroa-Gerstenmaier, F. J. Blas, J. B. Avalos and L. F. Vega, *J. Chem. Phys.*, 2003, **118**, 830–842.

106 N. F. Carnahan and K. E. Starling, *J. Chem. Phys.*, 1969, **51**, 635–636.

107 J. A. Barker and D. J. Henderson, *Rev. Mod. Phys*, 1976, **48**, 587–671.

108 D. B. McGuigan, M. Lupkowski, D. M. Paquet and P. A. Monson, *Mol. Phys.*, 1989, **67**, 33–52.

109 D. Frenkel, G. C. A. M. Mooij and B. Smit, *J. Phys. Condens. Matter*, 1991, **3**, 3053–3076.

110 J. I. Siepmann and D. Frenkel, *Mol. Phys.*, 1992, **75**, 59–72.

111 J. J. de Pablo, M. Laso and U. W. Suter, *J. Chem. Phys.*, 1992, **96**, 2395–2403.

112 B. Smit, *Mol. Phys.*, 1995, **85**, 153–172.

113 L. G. MacDowell, C. Vega and E. Sanz, *J. Phys. Chem.*, 2001, **115**, 6220–6235.

114 K. G. Honnell, C. K. Hall and R. Dickman, *J. Chem. Phys.*, 1987, **87**, 664–674.

115 L. G. MacDowell, *J. Chem. Phys.*, 2003, **119**, 453–463.

116 E. de Miguel, *J. Chem. Phys.*, 2008, **129**, 214112/1–6.

117 L. G. MacDowell and F. J. Blas, *J. Chem. Phys.*, 2009, **131**, 074705/1–10.

118 I. Benjamin, *J. Chem. Phys.*, 1992, **97**, 1432–1445.

119 J. S. Rowlinson and F. L. Swinton, *Liquids and Liquid Mixtures*, Butterworth, London, 1982.

120 C. Vega and L. G. MacDowell, *Mol. Phys.*, 2000, **98**, 1295–1308.

121 F. J. Blas and L. F. Vega, *J. Chem. Phys.*, 2001, **115**, 4355–4358.

122 J. K. Johnson, *J. Chem. Phys.*, 1996, **104**, 1729–1742.

123 P. Bryk, K. Bucior, S. Sokolowski and G. Zukocinski, *J. Phys. Condens. Matter*, 2004, **16**, 8861–8873.